Energy 278 (2023) 127820

Contents lists available at ScienceDirect

Energy

journal homepage: www.elsevier.com/locate/energy

Effect of the radial gap size on the deterministic flow in a centrifugal pump due to impeller-tongue interactions

J.M. Fernández Oro *, R. Barrio Perotti, M. Galdo Vega, J. González

Universidad de Oviedo, Área de Mecánica de Fluidos, Campus de Viesques s/n, 33204, Gijón, Asturias, Spain

ARTICLE INFO

Keywords:
Blades
Unsteady flows
Impellers
Stress
Centrifugal pumps
Interaction

ABSTRACT

The research on the flow in centrifugal pumps is quite broad and covers most of the relevant issues. However, most of the studies are focused on the steady behaviors and less literature is available for the dynamic interactions. Unsteady mechanisms for energy transfer and sources of impeller-tongue interaction can be identified in centrifugal pumps using the deterministic decomposition of the flow. Probably, the most important effect to be considered is the radial gap or spacing between the impeller exit diameter and the volute tongue radial location. The numerical dataset of a full 3D URANS model in a centrifugal pump has been employed to study in detail the effect of the radial gap size in the unsteady fluctuations of the velocity field within the pump, using the deterministic analysis as the main novelty. The numerical model developed by the authors has been already tested towards the prediction of the unsteady pressure field inside the volute, at the impeller exit. The new results presented here allow to see the impact of both geometrical and operating parameters on the flow discharge and momentum exchange. In particular, four different radial gaps (23.2%, 17.0%, 11.4% and 8.8% of the impeller diameter) operated at five different flow rates (from 20% to 160% of the nominal rate) have been numerically resolved and analyzed. The deterministic analysis reveals the major impact of the radial clearance on the blade-to-blade flow patterns within the impeller, especially at low flow rates. Unsteady viscous interaction induces radial velocity fluctuations that can be as high as a 40% of the time-averaged value. Moreover, this non-linear term can be perceived up to 1.5 times higher in the case of radial gap reductions from 23.2% to 8.8% of the impeller diameter. There is not a prevailing effect of the radial gap on that velocity component, and a pure temporal term dependence is found. On the contrary, the influence of the gap on the tangential component, responsible for the unsteady evolution of the impeller torque, is found to be the key parameter. Therefore, the fluctuations of the flow blockage are found to be the consequence of the impeller flow patterns and the fluctuations of the torque are to be assigned to the radial gap influence. All the post-processing routines have provided a precise picture of all the classic unsteady mechanisms involved: jet-wake pattern interaction, acoustic wave propagations and recirculating cells at off-design conditions. Hence, deterministic analysis is a useful tool to analyze the flow inside centrifugal pumps and it envisages the introduction of deterministic flow variables as objective functions for design optimization algorithms.

1. Introduction

Along the last decades, it can be estimated that roughly a 10% of the total energy consumption of the industrial sector in developed countries is devoted to transport fluids, see among others [1] or [2]. In particular, the use of centrifugal pumps is predominant for fluid pumping in most engineering processes. On the whole, centrifugal pumps constitute more than 85% of the world production of pumps. This is due to their suitable characteristics based on large head supplies, moderate-to-high flow rates, and the fact that they manage to keep the pressure peaks and transients below reasonable levels. In the present scenario of decarbonisation, and to favor sustainability and reduce carbon footprint of pumps, the requirement for improving their efficiency is mandatory, [3]. Also, with a continuous rise of the energy prices and recent concerns over the EU's ability to secure its energy supply, actions to promote the performance of the pumps are becoming relevant. Target plans for reduction in their energy consumption are currently emerging for maintenance, retrofitting and redesign, as stated in report by the [4]; so an improved knowledge on the behavior of the flow inside these machines has become critical in the last decades. A primary focus for global energy policy makers is to maximize the energy efficiency in pumping

* Corresponding author.
E-mail address: jesusfo@uniovi.es (J.M. Fernández Oro).

https://doi.org/10.1016/j.energy.2023.127820
Received 14 September 2022; Received in revised form 13 January 2023; Accepted 12 May 2023
Available online 13 May 2023

Nomenclature

b_2	Outlet impeller width, (m)
d_2	Outlet impeller diameter, (m)
d^*	Quotient of impeller diameter over reference one, $d_2 =$ 0.210 m, $d^* = d_2/0.210$, (−)
G	Radial gap, $G = 2r_T/d_2 - 1$, (−)
g	Gravitational constant, (m/s^2)
H, H_N	Head and nominal head, (m)
K	Pressure loss coefficient used in the numerical model, (Pa/(m^3/s)^2)
Q, Q_N	Flow rate and nominal flow rate, (m^3/s)
n_S	Specific speed, $n_S = \Omega Q_N^{0.5}/(gH_N)^{0.75}$, (−)
P	Pressure field in the pump, (Pa)
P^*	Normalized pressure, $P^* = P/(0.5\rho U_{tip}^2)$, (−)
r	Radial location, (m)
(R)	Rotor frame variables
r_T	Volute tongue radial location, (m)
t	Time, (s)
T_B	Blade passing period, (s)
U_{tip}^*	Corrected tip or shroud velocity, (m/s)
v	Flow velocity, (m/s)
v_r	Radial velocity, (m/s)
v_Θ	Tangential velocity, (m/s)
x	Position in the flow (vector)

Greek symbols

β_2	Impeller outlet blade angle, (rad)
Δ	Increment of a given variable
φ	Angular coordinate/position, (°)
Ψ	Head coefficient, $\Psi = gH/(\Omega^2 d_2^2)$, (−)
φ_N	Flow rate coefficient, at nominal conditions: $\varphi_N = Q_N/\Omega d_2^3$, (−)
Ω	Rotating speed, (rad/s)
κ	Turbulent kinetic energy, (J/kg)
ε	Turbulent kinetic energy dissipation, (1/s)
ρ	Density, (kg/m^3)
μ	Dynamic viscosity, (Pa·s)
θ, θ_{abs}, θ_{rel}	Angle, absolute and relative frames, (rad)
π	Quotient between length and diameter of a circumference, (−)

Mathematical operators

tan	Tangent of a given angle
$\widehat{,}$	Averaging of a given variable
$\rightarrow$	Vectorial variable
$',''$	Different terms in the deterministic analysis averaging

Acronyms

PIV	Particle Image Velocimetry
RMS	Root Mean Squared
SIMPLEC	Semi-Implicit Method for Pressure Linked Equations-Consistent
TE	Trailing Edge
URANS	Unsteady Reynolds-Averaging Navier-Stokes

systems, [5]; so scholars are encouraged to provide solid and deep guidelines for performance enhancement of centrifugal pumps. However, the analysis of the flow inside such turbomachines remains far from being solved. Their geometry consists of an outer volute with spiral geometry and a moving impeller with irregular channels, so centrifugal pumps have a complicated geometry. The first studies of this type of machine were focused on the analysis of its global performance considering the study of the basic characteristics of the flow through the mentioned geometry [6,7], or [8].

Due to the unsteady characteristics of the inside flow, a series of phenomena associated with this time-dependent behavior deserve particular attention. On top of that, the relative flow leaving the impeller is not uniform, due to the blades' boundary layers and the classic jet-wake pattern within the impeller passages. When such flow reaches the fixed parts of the machine (volute) it promotes a series of excitation phenomena, both tonal and in a broadband frequency range. On such frame, the radial gap between the impeller outlet and the volute tongue becomes a critical parameter that has revealed its major influence along the last decades, see Ref. [9] or [10] for a comprehensive and extended review.

Throughout the years, different scientific groups have analyzed the unsteady flow inside centrifugal pumps using different techniques. Both experimental and numerical approaches have been widely developed for that purpose. On the one hand, remarkable experimental works [11], among others, have analyzed intensively the dynamic forces in a centrifugal pump with a diffuser pump impeller. Other authors, specifically [12]; studied the variations that occurred in the flow field in the vicinity of the tongue using Particle Image Velocimetry (PIV). In recent decades, taking advance of the computing science development, many researchers have used numerical models to analyze unsteady flow fields inside centrifugal pumps, see for instance Refs. [13–15]; or [16]. In all these articles the authors analyze the impact of several geometrical parameters over the unsteady flow characteristics of centrifugal pumps using different numerical approaches. Some other recent contributions analyze the possibility of using centrifugal pumps as turbines in mini power plants [17]. Other authors investigate the behavior of these turbomachines when they pump high-viscosity liquids, as shown in the works of [18,19]. In those articles, the authors search for the optimization of geometrical parameters during the operation of these pumps with high viscosity liquids. More recently, the article by Ref. [20] targets the study on the cavitation phenomena in a centrifugal pump using numerical models.

Although there are several articles that study the flow inside these turbomachines, pump designers are always challenged in the search for a continuous improvement on the geometries. In terms of energy efficiency, blade redesigns based on secondary flow suppression [21], or bionic optimization of blade trailing edge for enhancement of energy consumption, [22]; are remarkable and with very advance proposals. The influence of the impeller tip clearance for the energy characteristics of mixed-flow pumps has been also studied using a novel entropy production analysis, [23]. Alternatively, optimized designs are currently being researched to reduce pressure fluctuations in the volute that cause undesirable vibrations. Precisely [24], have analyzed the influence of the rotational speed and flow rate conditions over the pressure fluctuations in a double suction centrifugal pump. In addition, the investigation of unsteady pressure fluctuations and methods for its suppression for a double suction centrifugal pump by Ref. [25] reported the convenience of staggered impellers. Obviously, in finding how to reduce such pressure fluctuations, it is necessary a deep knowledge of their origin and characteristics. A technique that allows discovering the nature of the fluctuations that occur in the flow is the deterministic analysis, started by Ref. [26]. Originally, it was conceived as a modelling tool for axial turbomachinery to address the unsteady contributions of rotor-stator interactions (deterministic stresses) in steady computations. Later, it was reoriented as a post-processing technique to identify the sources of viscous and potential interactions in unsteady data for multistage environments, [27]. In that same direction [28], introduced the methodology for the analysis of centrifugal turbomachinery,

performing the deterministic flow decomposition in both absolute and relative frames of reference. Recently, the authors have already successfully used this same methodology to study the interaction phenomena that occur between the impeller and the tongue of a single volute centrifugal pump, [29]. The impact of the operating conditions was revealed as a major contributor for the evolution of unsteady sources on the impeller passages. Off-design flow rates have been found to be particular susceptible for major unsteadiness, with significant interaction between the detached flow at the blades pressure side and the blockage induced by the volute tongue. On the contrary, the volute flow structures were observed as practically absent of deterministic stresses. Additional conclusions on the unsteady transport of turbulent structures were also derived from the deterministic framework. A limit on the impeller-volute interaction was desirable for the blades, either optimizing the blade profile close to the trailing edge or modifying the gap distance between the impeller outlet and the tongue. In the present article, the deterministic analysis is used for the first time to study the effects of the radial clearance between the impeller and volute in a centrifugal pump. The basic objective and main goal of the paper is the identification of the physical phenomena responsible for the establishment of rotor-tongue interactions and how these mechanisms are influenced by the operating conditions for different radial gaps. The flow decomposition in both absolute and relative frames of reference will allow to reveal secondary flows and analyze viscous flow patterns that penalize the energy efficiency of the pump. Regarding such kind of dynamic interaction, the deterministic flow decomposition has shown its potential and might help in the recognition of the primary sources of the so complex flow behaviors inside a centrifugal pump. The present study combines the use of an already existing numerical model with the calculation of the deterministic components to handle such problem.

2. Description of the model

2.1. Geometry of the pump

The pump used in this study is a commercial centrifugal pump with a single suction and a volute casing. The impeller has 0.2 m in outer diameter and it is equipped with 7 twisted blades with a logarithmic shape in their mean line and an exit angle of 29 deg (Fig. 1). The outlet width of the impeller is 16.9 mm. The reference values of this impeller at nominal conditions are $Q_N = 0.015$ m^3 s^{-1} and $H_N = 12.9$ m, which result in a non-dimensional specific speed of $n_s = 0.52$ at $\Omega = 1620$ rpm. The tip of the volute tongue is located at a radial distance of $r_T = 0.117$ m from the center of the impeller, thus resulting an impeller-to-tongue radial gap of 17.0% referred to the outer diameter of the impeller.

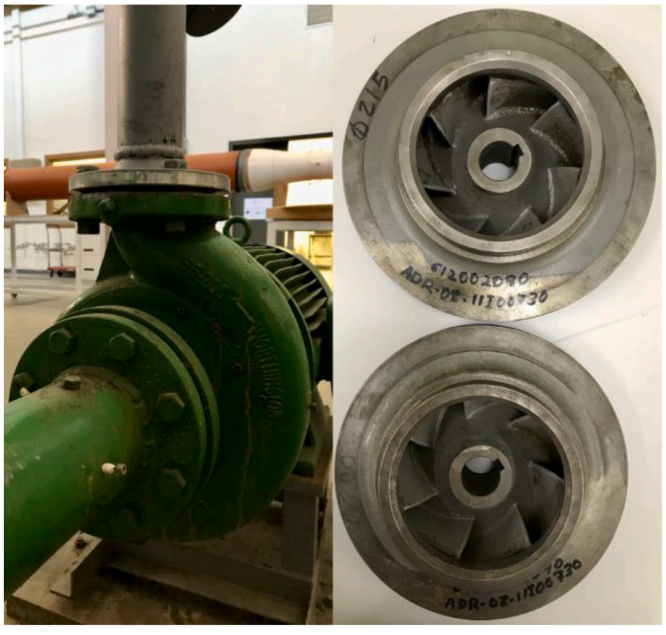

Fig. 1. Test pump (left) with a detail of the impellers of diameter 0.215 m and 0.2 m (right).

The global performance of the pump and several unsteady flow features have already been investigated at nominal operation and at off-design conditions in previous works by the authors [9,30], or [31]. Also, as a natural evolution of the previous studies and complementing them [10], showed a detailed analysis of some typical flow patterns near the tongue region of the volute and also an evaluation of the unsteady radial load acting on the impeller at blade-passing frequency as a function of the radial gap and of the flow rate. The pump can be equipped with three additional impellers that can change the radial gap between 23.2% and 8.8% of the impeller outlet radius, as shown in Table 1. The effect of this gap variation on the deterministic stresses that are correlated to the interactions between the impeller and the volute tongue will be the main topic of the following sections.

2.2. Numerical model for the unsteady 3D flow

A numerical model based on the pump geometry, as described in the previous section, was developed in order to compute the unsteady flow. For this purpose, the numerical domain was divided into four separate volumes: impeller, volute, and pipes (inlet and outlet). The numerical volume of the impeller was extended to a radius of $r = 0.112$ m to be able to enclose the four diameters shown in Table 1. In consequence, only this volume had to be changed when varying the impeller diameter, thus avoiding any geometrical or mesh distortion in the remaining volumes, as seen in Fig. 2. A pair of grid interfaces, one of them located at the exit of the impeller volume (rotating), and the other one located at the inlet of the volute volume (stationary), were created to transfer the flow field data between the volumes (see Fig. 2). Additionally, the frontal and back walls of the casing were also included in the numerical volume of the impeller to account for the viscous friction of the flow between these walls and each side of the impeller, as can be seen in the full numerical model presented in Fig. 3.

A structured mesh of prismatic cells was used for both pipes at the inlet and at the outlet of the pump whereas an unstructured mesh of tetrahedral cells was adopted for the remaining volumes (see Fig. 3), with particular refinement close to critical zones like the blades leading edge and the volute tongue. A mesh independence analysis was carried out with one of the impellers at the highest flow rate (160% of rated flow). This analysis showed that a mesh size of about 800,000 cells (70,000 cells in each blade passage) was enough to preserve numerical uncertainty below 4% even for the unsteady variables. Although this mesh size is still not adequate to calculate boundary layer variables, it is fine enough to perform a deterministic analysis of the velocity fields as shown in previous numerical approaches for similar geometries, Fernández Oro et al. (2011) y (2019).

The operation of the pump with water ($\rho = 998.2$ kg m^{-3}; $\mu = 10^{-3}$ Pa s) was predicted with the four impellers by solving the Reynolds-Averaged Navier-Stokes equations for unsteady flow (URANS) and the continuity equation with the commercial software ANSYS-Fluent®. Second order discretizations were established for convection and diffusion terms and also for time dependent terms. The SIMPLEC

Table 1
Radial gap as a function of the impeller outlet diameter.

Impeller diameter, d_2 (m)	$d^* = d_2/0.210$	Radial gap, G (%)
0.190	0.905	23.2
0.200	0.952	17.0
0.210	1.000	11.4
0.215	1.024	8.8

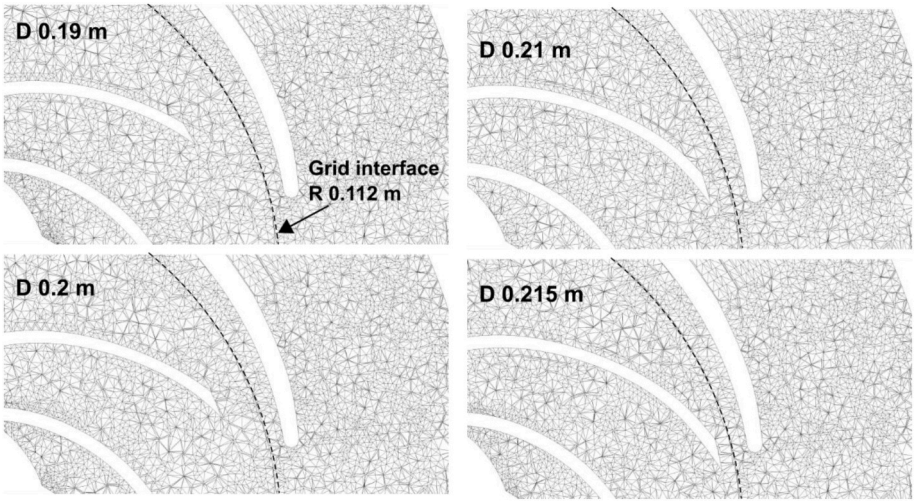

Fig. 2. Transversal cut of the mesh at impeller mid-span for the four impellers. The position of the grid interface that allows the relative motion of the impeller is also indicated.

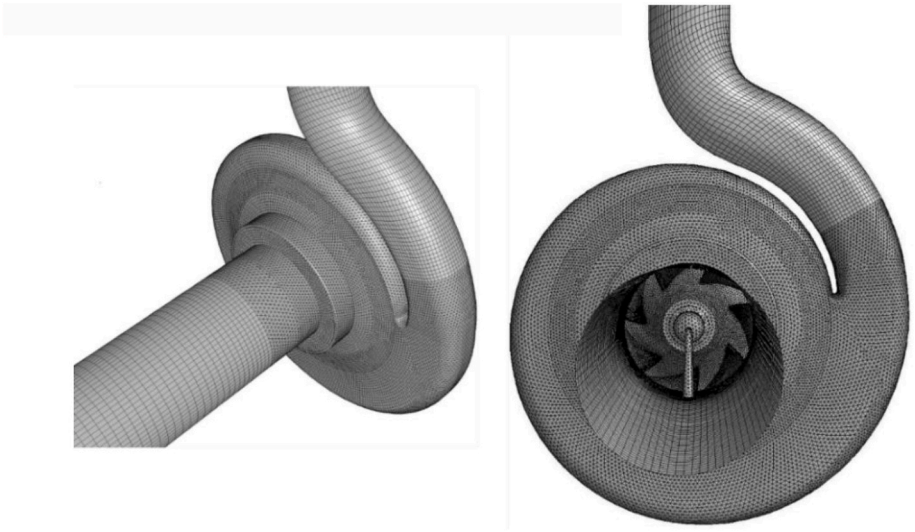

Fig. 3. 3D view of the volume mesh with a detail of the impeller inlet showing an inlet guide vane.

algorithm set the coupling between velocity and pressure fields. The κ-ε RNG turbulent model was used for turbulent closure (after testing other models with no significant differences found) together with the usual velocity profile based on a logarithmic law in order to compute the flow in the boundary layer (standard wall function). A magnitude of the y + between 100 and 190 was computed on the surface of the blades for all the impellers and flow rates tested. A constant total pressure was imposed as inlet boundary condition. At the exit of the outlet pipe a static pressure boundary condition proportional to the local dynamic pressure was imposed by a coefficient K (outlet-vent type). The particular values of K, required to establish the different points of operation, were deduced from the performance curves previously obtained in laboratory tests [10].

The rotation of the impeller mesh with respect to the stationary meshes of the inlet pipe and the volute was set by grid interfaces (see Fig. 2) and the sliding mesh approach supported in ANSYS-Fluent®. A full impeller rotation was calculated in 224 time steps with a time interval of $1.65{\cdot}10^{-4}$ s between two consecutive time steps. This resulted in a total amount of 32 time steps per single blade passing period that caused angular displacements of the impeller evenly distributed every 1.6 deg. At least 10 impeller revolutions were required to ensure a stabilized flow regime with a convergence criterion below 10^{-5} for the scaled residuals. Additional 32 time steps were run and post-processed after these calculations to get the results that are shown in the following sections.

The value of 32 time steps per blade passing period was selected after testing 8, 16, 32 and 64 time steps. The results of this time step sensitivity analysis are shown in Table 2, where the outlet volumetric flow Q, the head H and the normalized amplitude P^* of the static pressure at blade-passing frequency in a position located 20 deg. from the tip of the tongue were selected as reference variables. As seen, the variations observed with 32 time steps are below 4% for the most different comparison with most values below 1% even for the unsteady variable P^*, and therefore this value was adopted for the numerical calculations in

Table 2
Results of the time step sensitivity analysis.

Time steps	Q (m^3/h)	ΔQ (%)	H (m)	ΔH (%)	P^* (−)	ΔP^* (%)
8	86.52		10.82		0.0509	
16	87.10	0.67	10.93	1.02	0.0425	16.45
32	87.43	0.38	11.00	0.64	0.0409	3.94
64	87.65	0.25	11.05	0.45	0.0410	1.06

order the keep the computational cost below an acceptable level.

The numerical model used in this study was validated in previous investigations by the authors where the focus was set on the unsteady pressure fields, (see for instance Refs. [10,16]. As an example of this validation, Fig. 4 shows a comparison between the experimental measurements and the numerical predictions of the non-dimensional performance curve, observed in the experiments from the impeller with d* = 0.905 (lower limit) to the impeller with d* = 1.024 (upper limit). As observed, the contrast between the experimental and numerical performance curve shows a good qualitative and quantitative agreement, with marginal differences around 5% for a wide range of operation. It must be noted that the experimental curves represent the operation of three of the four impellers for clarity, whereas all the impellers are represented for the numerical data. The agreement between the different datasets can be considered also as satisfactory. There is an efficiency improvement as the diameter of the impeller increases and the predicted values lie within the range observed in the experiments for most of the flows.

The amplitude of pressure fluctuations at blade-passing frequency round the impellers with d* = 0.905, d* = 0.952 and d* = 1 are presented in Fig. 5 for three of the tested flow rates: 60%, 100% and 160% of rated. The distribution of the pressure amplitude round the impeller shows some degree of modulation that is the result of the combination of the jet-wake mechanism and of the acoustic wave propagation resulting from the interaction of the blades with the volute tongue, which is especially clear for the lower values of φ. As seen, the blade-tongue interaction is reinforced when deviating from nominal operating conditions, especially in the narrow zone of the volute (φ < 30 deg) and at the highest flow rate, where this fluctuation can be up to 3.5 larger than at nominal conditions. The reduction of the impeller-tongue gap also reinforces this fluctuation: for example, the maximum fluctuation in the tongue region at 60% flow rate is 50% larger for the impeller with d* = 1 when compared with that observed when d* = 0.905, and it is 80% larger at the highest flow rate. As seen in Fig. 5, comparison between the numerical and the experimental pressure fluctuation data gives a satisfactory agreement, even at the tongue region, where this interaction is more noticeable.

2.3. Numerical dataset

Five different flow rate conditions, ranging from 20%Q_N to 160%Q_N, have been considered for all the diameters of impeller tested. This implies a total numerical dataset with up to 20 numerical executions in a non-stationary routine. For every execution, 32 files including all the velocity components, the pressure fields and the turbulent magnitudes were stored in different sections of interest to analyze the unsteady flow

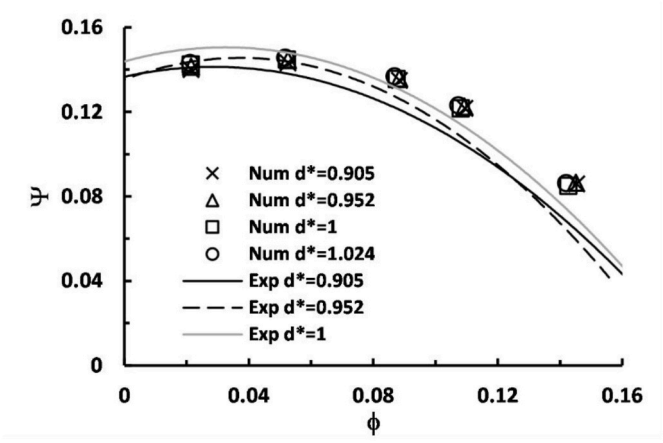

Fig. 4. Numerical and experimental comparison of the non-dimensional performance curve, adapted from Ref. [10].

in a blade passing period of the impeller. For further post-processing, both radial and tangential velocities were made non-dimensional with reference values corresponding to the typical throughflow velocity (eq. (1)) and the impeller tip velocity (eq. (2)):

$$v_r = Q / (\pi d_2 b_2) \tag{1}$$

$$U^*_{tip} = 0.5\ \Omega d_2 - v_r / \tan \beta_2 \tag{2}$$

Table 3 summarizes the typical values obtained for the five operating conditions executed in the study. This normalization will allow a more representative comparison between the results in the following sections. The radial velocities are made non dimensional using the characteristic radial velocity associated to every operating flow rate. Note also that the diameter d_2 of 210 mm has always been considered as the reference. Complementarily, the tangential velocities have been made non-dimensional with a modified tip velocity that takes into account the circumferential projection of the outflow velocity at the impeller (thus, function of the flow rate).

3. Deterministic decomposition and primary flow variables

In unsteady environments of turbomachinery, the velocity fields can be decomposed in a steady component (time-averaged) and a fluctuating term that includes both turbulent and periodic contributions. This second term, after removing turbulence with a phase-averaging operator, can be further decomposed using the deterministic analysis. In essence, the remaining unsteadiness can be treated as a spatial gradient generated in the impeller that it is steady in the relative frame but rotating unsteadily in the absolute frame. This can be mathematically expressed as follows:

$$\tilde{v}(\vec{x},t) = \bar{v}(\vec{x}) + v'(\vec{x},t) = \bar{v}(\vec{x}) + v''^{(R)}(\vec{x}') + \hat{v}(\vec{x},t) \tag{3}$$

Since the present numerical database for study is obtained from a URANS simulation, the unsteady results are already absent from turbulent fluctuations: i.e., they are fully deterministic. In equation (3), the spatial gradient of the blade-to-blade non-uniformities, $v''^{(R)}$, is complemented with a pure unsteady term, $\hat{v}$, that addresses the impeller-tongue interactions and that it is regarded as a totally nonlinear term. Note that $\vec{x}'$ considers the change in the frame of reference required for the tangential component: $\theta_{abs} = \theta_{rel} + \Omega t$. More details on the decomposition procedure and theoretical basis of the model can be found in Ref. [29].

3.1. Unsteady radial velocity

The influence of the radial gap on the flow discharge in the impeller is illustrated in Fig. 6. The maps show the non-dimensional distribution of the radial velocity at the impeller exit. All the flow rates analyzed are represented for the case with the largest radial gap (left) and for the smallest gap (right). For a better representation, the circumferential coordinate has been extended and drawn in the x-axis. Note that the position of the volute tongue has been identified with a red vertical line at 11.8 deg in all the maps. The white dashed lines indicate the impeller width. All the distributions correspond to one instantaneous snapshot of the 32 time-steps evolution for the blade passing period.

These results reveal how the flow discharge at the impeller is blocked at different flow rates when the radial gap to the volute tongue is significantly reduced. At lower flow rates, it is a common feature the existence of flow recirculation in the upper clearance of the impeller (close to the shroud). At 60% and especially at 20%, there are recirculation cells with small and even negative values of radial velocity in that zone, while in the inner part (close to the hub) positive values of velocity are observed, especially for positive angles where the volute is narrower. Also, the distribution of radial velocity on the blade surfaces is not symmetrical but displaced downwards, towards the hub zone. This is

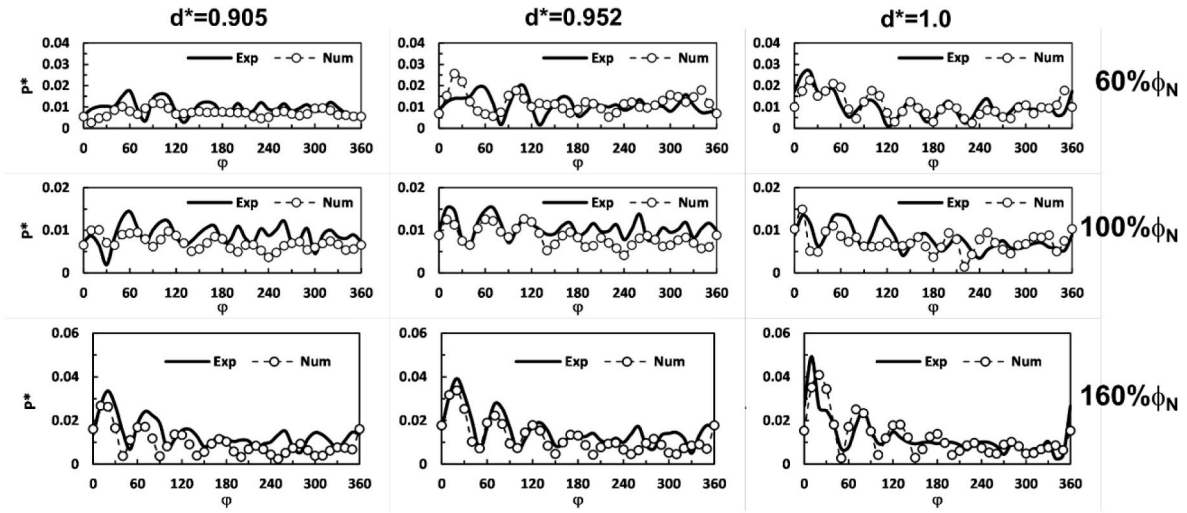

Fig. 5. Pressure fluctuations at blade-passing frequency round the impellers with d* = 0.905, d* = 0.952 and d* = 1 for three flow rates, adapted from Ref. [31].

Table 3
Numerical dataset and reference parameters for the nominal impeller.

K	φ/φ_N (%)	Q (m^3/s)	v_r (m/s)	U^*_{tip} (m/s)
3.0	160	0.024	2.26	12.88
9.0	120	0.018	1.70	13.90
16	100	0.015	1.41	14.41
50	60	0.009	0.85	15.43
300	20	0.003	0.28	16.45

especially evident in the central zone of the maps at 20% and 60% for the two gaps, where the blocking effect caused by the tongue is more significant. On the contrary, in the case of high flow rates, this flow trend is inverted with outgoing flows entering the volute mainly close to the shroud. This is more significant at 160% in the central zone of the map (again where the effect of the tongue is more pronounced), with positive radial velocities at the upper mid width of the impeller. At 160%, there are two adjacent zones on both sides of the tongue, more noticeable for the smaller gap, where there is a significant change in the sign of the radial velocity.

In addition, the classic jet-wake pattern in the blade-to-blade structure is clearly visible in all the cases, especially with flow rates higher than 100%. All the passages are quite similar with a clear circumferential symmetry. Even for 20% and 60% the flow pattern is mostly preserved, especially where the volute is wider (negative values of the angular coordinate). However, in the blade approaching the tongue, an extensive zone of negative radial velocity is produced by the blockage of the predominantly tangential flow recirculating from the diffuser area towards the tongue. This causes the impeller outflow to concentrate in a very narrow and downward outlet section. The severe impact of low flow rates in the impeller discharge is thus remarkable in that pattern. Also note that, at 20%, there is always a part of the passage partially blocked during the complete blade motion, reaching the maximum blockage when it is close to the tongue. When the passage is partially released after passing along, the zone with low radial velocity is recovered.

An opposite effect is seen for high flow rates, 120% and especially 160%. It is observed a higher radial velocity associated to the pressure side of the incoming blade towards the tongue and related to the higher exit angle of the flow. This is provoked by the recirculation established between the initial narrow area of the volute and the outlet diffuser which favors the flow discharge from the passage.

3.2. Time-averaged tangential and radial velocities

The variation of the outlet tangential velocity is responsible for the momentum transfer in the centrifugal impeller. To analyze the impact of the gap size on that component, the time-averaged value of the circumferential velocity is represented now in Fig. 7 (right) at the midspan position of the impeller outlet. The red line identifies the

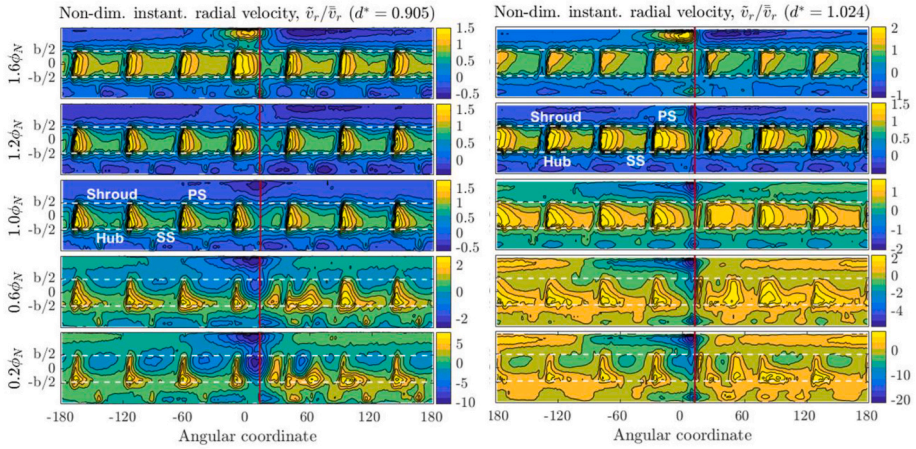

Fig. 6. Unsteady radial velocity at the impeller exit as a function of the flow rate: Radial gap G = 23.2% (left) vs Radial gap G = 8.8% (right).

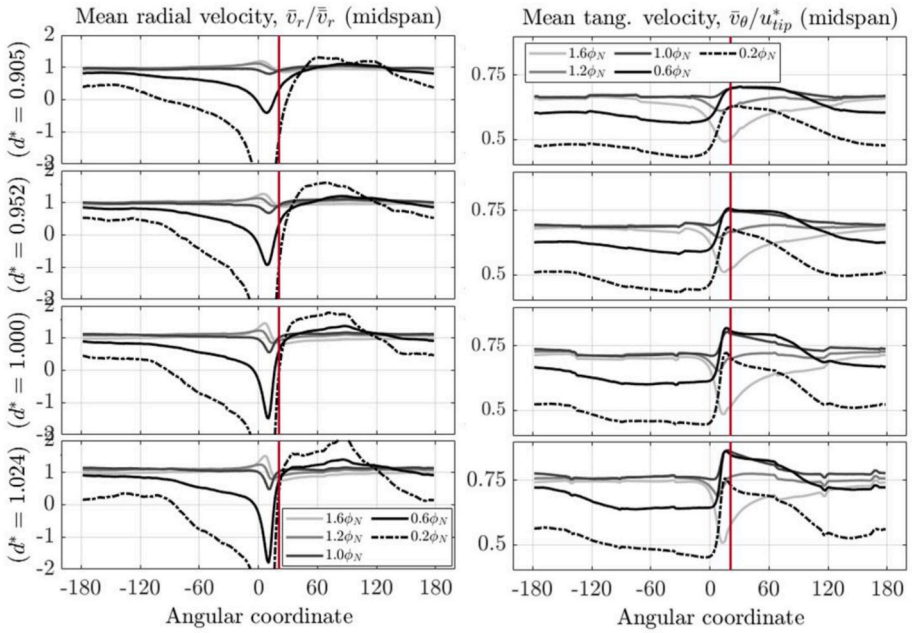

Fig. 7. Time-averaged velocities at the impeller exit as a function of the radial gap (highest on top, lowest on bottom): Radial velocity (left) vs tangential velocity (right).

angular position of the volute tongue. The evolution of the meantime velocity distribution with the radial gap is shown for the different flow rate conditions. Since the time-averaging is performed in the absolute frame, the contribution of the blade-to-blade gradients is smeared out. As a reference, similar results for the radial velocity are also shown in the figure (left).

This type of representation clearly reveals the impact of the tongue discontinuity on the flow patterns. In the case of the radial velocity, major differences are due to the flow rate conditions, rather than the influence of the radial gap size. Note that at lower flow rates (20% and 60%), high negative radial velocities are found in the tongue region due to the blockage effect which are "recovered" after passing that obstruction. In general, the influence of the flow rate is more pronounced than that of the gap, but both are negatively combined at low flow rates and reduced gaps. The effect of the blocking vortex starts to be developed from −120 deg to 120 deg approximately. It can also be observed that, after passing the tongue, there is a partial unblocking along the volute that generates a significant increase in the radial component of the velocity. This is linked to the constriction of the outflow in a smaller section, which results in a significant rise in the radial velocity after the initial drop, especially at low flow rates as previously discussed. On the other hand, at large gaps and high flow rates, the distribution is remarkably uniform (there is little impact of oscillation).

Similar effects are also observed for the tangential velocity. A clear change in the circumferential distribution is revealed between low flow rates (black curves) and medium and high flow rates (gray curves). A higher blockage (either by low off-design conditions or by lower gap) implies lower tangential velocities (under-turning) before the tongue, which experience a sudden rise when impinging the tongue. This should have an implication on the direction of the average force on the impeller. In addition, for low flow rates (20% and 60%) the velocity angle is small, and the stagnation point at the tongue is located on the outlet side of the pump; therefore, the flow is "dragged" to recirculate between the impeller and the volute back to the narrow zone of the volute, inducing an increment of the tangential velocity as it approaches the tongue. At high flow rates the effect is just the opposite: the outlet angle is high, and the stagnation point is located in the inner zone of the tongue, so that the flow tends to generate a small recirculation between the impeller-volute gap and the outlet, thus decreasing the tangential component by the partial blockage of the flow that occurs in this area. Fig. 8 shows the displacement of the stagnation point at off-design conditions: low flow rates (left) vs high flow rates (right). Velocity vectors (absolute in the volute; relative within the impeller) are superimposed to the static pressure contour map.

As a step forward, a certain correlation might be extracted between the velocity components and both radial force and torque over the impeller, from the point of view of averaged values. In the case of the radial velocity, it is evident that the lower the uniformity of this distribution around the impeller, the higher the radial force generated. This is confirmed when the stationary force over the impeller is calculated as a function of the flow rate, even pointing out that the force will increase as the gap is reduced. Previous results of the authors [10] have determined that the stationary force has both positive x-coordinate and y-coordinate components, with an angle of about 80° with respect to the horizontal axis, in the case of low flow rates (20% and 60%). This can be related to the zone of high tangential velocity observed between 20 deg and −120 deg (which is, in turn, associated with the low-pressure region shown in the pressure maps of Fig. 8) and the low tangential velocity zone from −120 deg on (associated now with high pressures). This would tend to cause the force previously observed from below and to the right, oriented in a coherent direction. At high flow rates (120% and 160%), the angle of the force is about −60 deg to −70 deg, according to previous calculations, thus showing positive component in the x-coordinate and negative in the y-coordinate. This can be related to the change of trend of the radial velocity in the vicinity of the tongue (it goes from decreasing with low flow rates to increase slightly with high flow rates), inducing a change in the angle of the force close to 180 deg.

Regarding the tangential component, and up to the authors' knowledge, the average torque increases as the flow rate increases and, for the same flow rate, increases slightly as the gap decreases. These effects are coherent with the evolution of the tangential velocity in Fig. 7 (right).

4. Deterministic components

In this section, the velocity terms derived from the deterministic analysis are presented in detail. Firstly, the flow structures in the relative

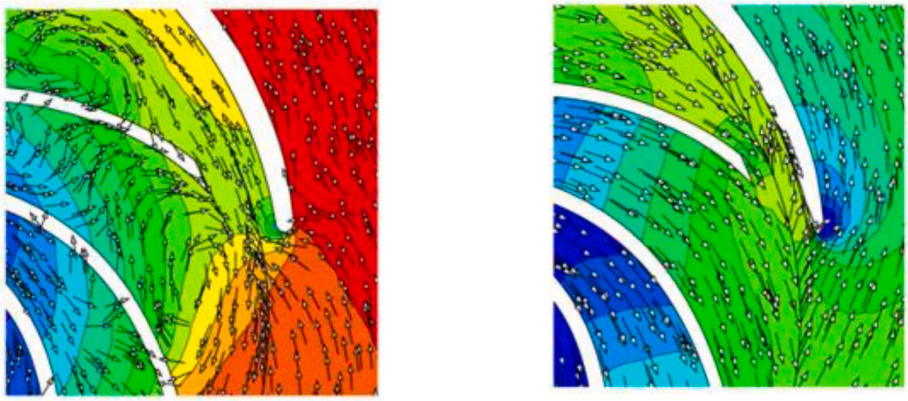

Fig. 8. Instantaneous flow field patterns in the vicinity of the volute tongue. Static pressure maps and velocity vectors: relative (at the impeller) and absolute (at the volute). a) 20% flow rate conditions for d* = 1.00 (left); b) 160% flow rate condition for d* = 1.024 (right).

frame are presented in the initial subsection. Due to the periodicity of the spatial gradients, only two blade pitches are presented (duplicated for convenience). Following, the pure temporal component responsible for the impeller-tongue interaction is shown in the second subsection. To conclude, the time-averaged impact of that non-linear component is described in terms of RMS values in the final subsection.

4.1. Blade-to-blade flow patterns

The blade-to-blade flow component is observed in the relative frame in Fig. 9 at the impeller outlet. As in previous sections, the circumferential ring corresponding to the radial exit of the impeller has been extended and drawn planar in the representation. All the cases corresponding to the whole dataset of the present investigation are included for the best comparison. Note that this component represents the "oscillation" in the radial velocity due to the passage of the blades: the negative and positive values represent fluctuations with respect to the mean value shown in the previous figures.

A singular feature is the presence of a series of nodules linked to the mid-passages of the impeller and observed in the bottom part close to the hub (below the impeller outlet rim). Note that this effect is particularly associated with large gaps and occurs at all flow rates. This pattern was already visible in the instantaneous maps in Fig. 6, but now it is revealed that its presence is totally related to the impeller geometry in the relative frame of reference. Effectively, the impeller has reinforcement fins at the back for mechanical balance, so this flow structure simply corresponds to the relative flow that, between fins, tends to form cells that rotate in the opposite direction to the impeller.

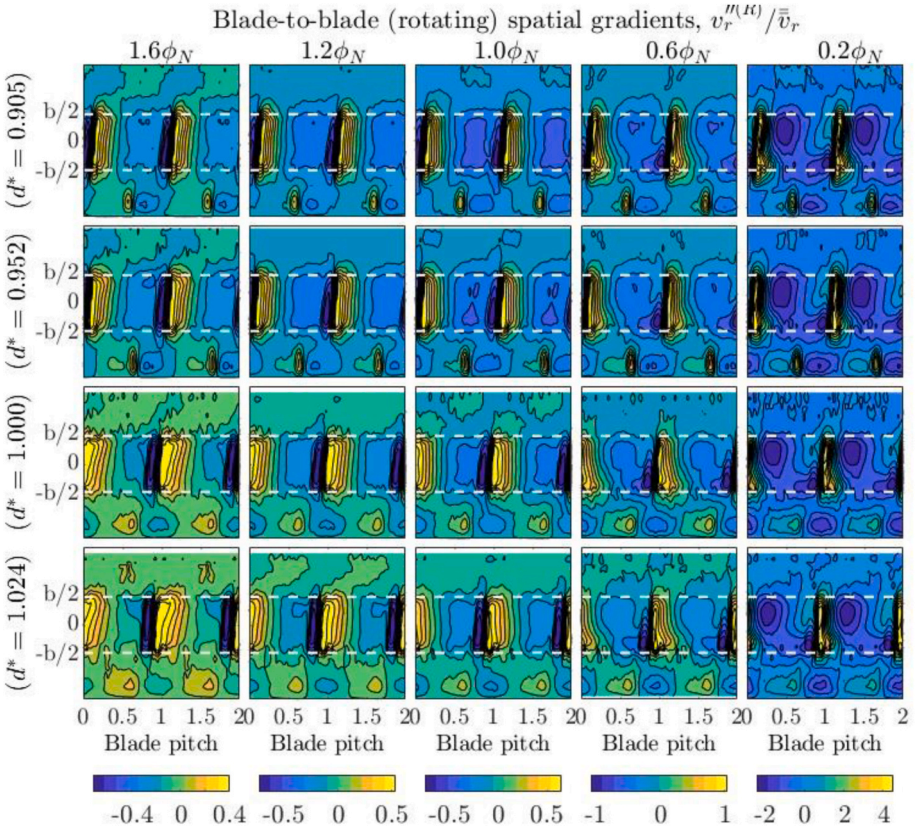

Fig. 9. Blade-to-blade gradients of the radial velocity in the impeller relative frame. Impact of the off-design conditions and the radial gap size on the flow patterns within the impeller passages.

However, the most characteristic distribution in the maps is the typical hydrodynamic load on the blades, obviously limited to the outlet width of the impeller (between the dashed lines) and usually referred to as jet-wake pattern. Note that in the present dataset, it is well appreciated for medium and high flow rates. For a given flow rate, it becomes clear that the region with high positive fluctuations on the pressure side of the blades becomes more and more extended in the direction of the pitch with the wake narrowing as the impeller diameter increases. This is nicely evident when comparing the results of impellers $d^* = 0.905$ and $d^* = 1.024$ at 160% of the nominal flow rate. This phenomenon can be associated to the length of the blades: as they are longer, the ability of the detached flow produced at the leading edge to reattach to the blade wall is favored when the impeller is larger in diameter. Logically, this effect is less noticeable at nominal flow rate when the flow inlet angle matches the geometrical one and, hence, the detachment is minimized (although it can be partially perceived in the figure).

At low flow rates, 60% and especially 20%, the severe blockage in all the passages is clearly revealed. It is noticeable that, apart from the major low-velocity zone attached to the shroud and already observed in previous figures, another smaller low-velocity zone appears on the suction side displaced towards the hub, interacting with the main deficit. As before, if the diameter of the impeller is increased, these phenomena tend to be attenuated. These secondary flow structures can be associated to the classic recirculation cells presented in the technical bibliography at the impeller outlet, see for instance Ref. [8]. For the present centrifugal pump, the cell closer to the hub is smaller while the larger cell is formed near the shroud towards the leakage zone.

The fluctuation component in the moving frame for the tangential velocity is shown at the midspan plane of the impeller outlet in Fig. 10. In this case, the positive oscillations (overturning) are intensified as the radial gap is reduced. As expected, as the impeller diameter increases and, with it, the drag component, so does the tangential component of the relative velocity. Once again, high tangential velocities are observed in the jet zone while low (negative) velocities are established in the wake

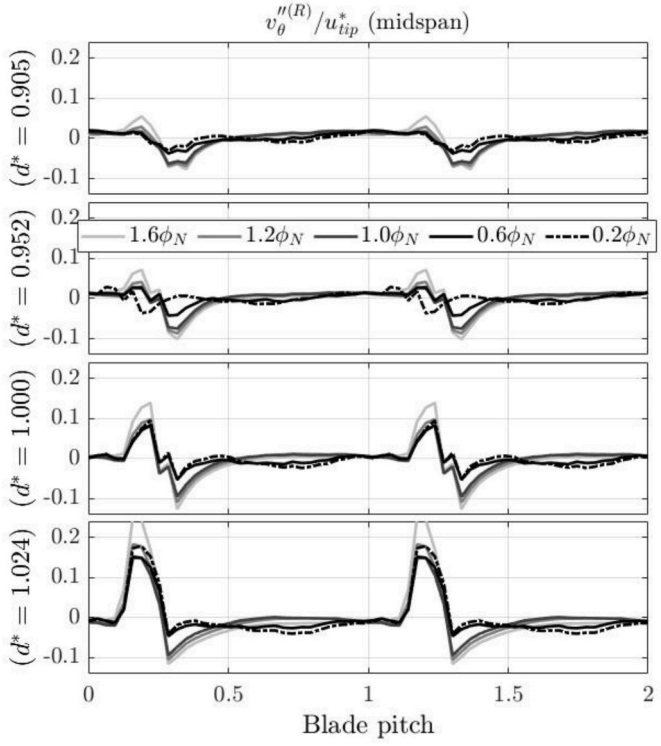

Fig. 10. Blade-to-blade gradients of the tangential velocity at the midspan of the impeller outlet section. Comparison of the influence of the radial gap size and operating conditions.

region. Note also that the impact of the flow rate is marginal for this component (only the off-design condition at 20% of the nominal flow rate is deviated).

4.2. Unsteady impeller-tongue interactions

In this part dealing with the dynamic flow interaction between the flow leaving the impeller and reaching the volute tongue, the component responsible for the viscous, unsteady interaction is analyzed in Fig. 11 at the midspan of the impeller out plane (x-axis of the contour maps), showing the influence of the flow rate for the largest (left) and the smallest (right) radial gap. In each map, the temporal variation of this component as a blade is passing by is observed along the y-axis of the contour maps. Results are shown for the radial velocity, where this phenomenon is more pronounced. The largest fluctuations are produced by the viscous interaction between the jet-wake flow and the blockage of the tongue (red line). At very low flow rates (20%), this fluctuation is again much more intense (up to +/− 4 times the mean radial velocity value). Also very relevant is the change that occurs when the impeller diameter is modified, especially at low flow rates, where the maximum amplitude is multiplied by a factor 1.5. As expected, the case of the nominal flow rate presents the lower interaction, especially in the case with the larger gap. As the gap is reduced, the case with less interaction is shifted towards the situation with 120% flow rate. Note that even at nominal conditions, this viscous interaction can be as high as 40% of the meantime radial velocity in the case of $d^* = 1.024$. As we move to the external opposite circumferential position with respect to the tongue (−180 and 180 deg), the interaction is progressively attenuated, though refraction mechanisms of the interaction waves are clearly observed.

Classic on this particular topic, as for instance Ref. [32] establish that the evolution of an unsteady variable within a centrifugal pump is generally associated to (1) hydraulic blade-vane interaction due to the jet-wake phenomenon or (2) blade-vane acoustic interaction. The first effect, responsible for an alternating pattern of ups and downs in the value of the variable, is coherent with the oscillations retrieved in the vicinity of the tongue. This is a local effect which can be perceived along any vertical line of the contour maps, especially for low flow rates in the range between 0 and 60 deg of the angular coordinate. On the other hand, the second mechanism produces an interaction wave that can be assumed to propagate as a planar wave along the volute at the speed of sound (i.e., almost instantaneously). As it propagates along the length of the volute, the wave is attenuated, losing intensity due to the enlargement of the cross-section. Moreover, when the interaction wave is generated, in some areas of the impeller periphery the jet-flow pattern contributes to enhance the wave, while in other zones, the wake deficit reduces its modulation. This can be observed in all the maps through horizontal lines at any given instant of the blade passing period. Up to seven traces can be observed in the maps regarding to the modulation of the acoustic pressure wave due to the jet-wake structure in the impeller blades. Once again, this is more evident at off-design conditions. For instance, at 20% or 60%, a plot of the values at a horizontal line at $t/T_B = 0.7$ would reveal that the maximum amplitude is generated, as expected, at the tongue; and that its effect is still appreciable along the positive values of angular coordinate, though in a progressive decay. After coming back from −180 deg, and going onwards on the angular coordinate, it is also clear how the decay is preserved until reaching the tongue again from the left.

Another significant characteristic is the delay observed in the interaction when the impeller diameter is increased. Comparing the same flow rate condition (for instance, 160%Q_N) for two different impeller diameters, the map distribution of the larger impeller is displaced upwards with respect to the shorter one. This feature, especially evident in the tongue area, is a consequence of the longer blades and thus, the elapsed time required for the trailing edge to reach and interact.

Finally, it is also remarkable an interesting lag in the distribution of the interaction between low and high flow rates. In particular, a direct

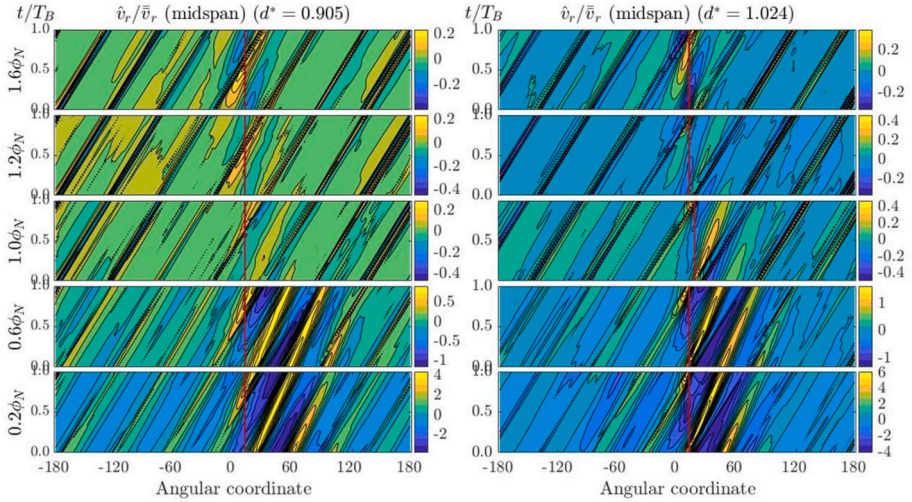

Fig. 11. Pure temporal term of the radial velocity responsible for impeller-volute interactions. Comparison of largest (left, d* = 0.905) and smallest (right, d* = 1.024) radial gap size with the flow rate.

comparison of the tongue area between 20% and 160% flow rate conditions reveals that the interaction cells are reversed. In the lowest flow rate for the small impeller, the positive cell is placed above the negative cell, while this trend is inverted in the case of the highest flow rate. This observation agrees perfectly with previous predictions of an acoustic model developed for centrifugal pumps by the authors' research group [33,34] in which it was concluded that the interactions at low and high flow rates can be modeled with complementary types of acoustic point sources being out-of-phase by a 180 deg delay approximately.

4.3. Time-averaged impact on the pump performance

In order to provide a big final picture of the viscous interaction within the impeller, a close view to the vicinity of the volute tongue is now shown in Fig. 12. For convenience, the unsteady character of the interaction component for the radial velocity has been reduced to a time-averaging contribution computing the RMS value of the fluctuation. This representation allows to address the "averaged footprint" of this source of unsteadiness. As already discussed above, the effect of the flow rate is more relevant than the effect of the gap, since the flow detachment and the recirculation observed on the pressure side of the blades at low flow

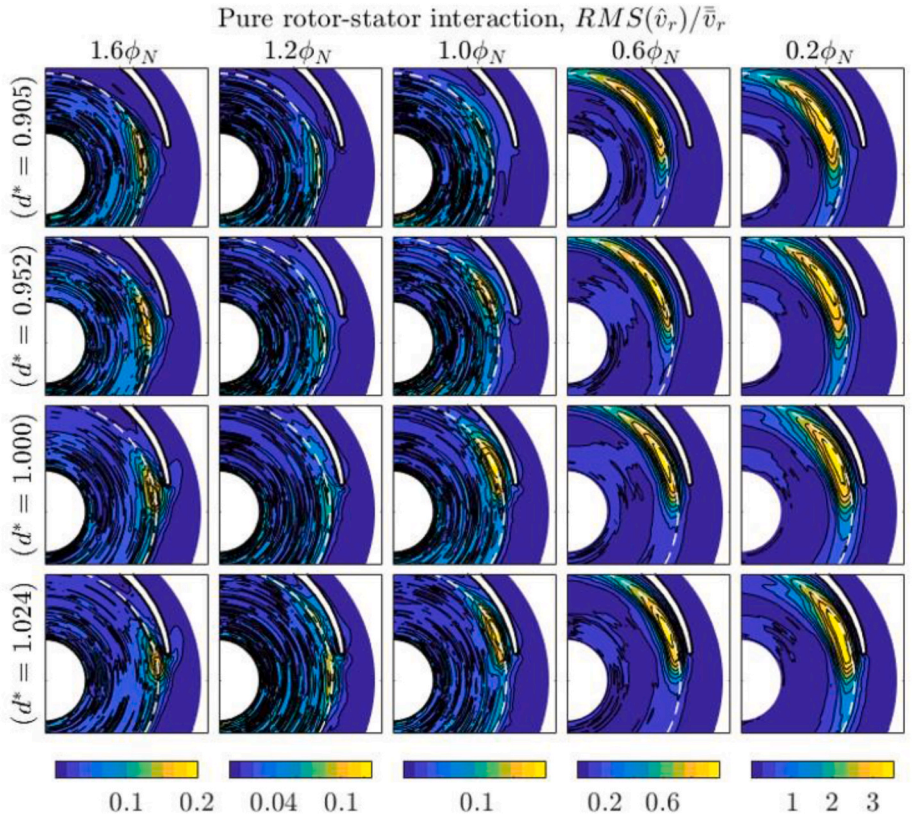

Fig. 12. RMS value of the pure temporal term in the blade-to-blade midspan plane for the radial velocity. Impact of the off-design conditions and the radial gap size on the flow patterns.

rates interacts dramatically with the tongue. In other circumferential positions of the impeller, this behavior is not observed. At high flow rates, the interaction zone is also observed, but it is much weaker (one order of magnitude), with quite smaller size and more aligned with the tongue (at low flow rates it goes upwards).

These results can be complemented with temporal evolutions of the static pressure in Fig. 13. In particular, the comparison for three different flow rate conditions is provided for the impeller with d* = 1. At low flow rates, the instant with the minimum pressure in the tongue area corresponds to $t/T_B = 0.59$ on the inner side of the tongue. Furthermore, the extension of such low-pressure region is considerable and related to the recirculated portion of flow rate that migrates back to the impeller. On the other side, for the higher flow rate, the pressure maps show that the minimum pressure is also reached for the same instant, but located close to the tongue edge and associated to the recirculation that now is going outwards. A moderate influence of the impeller diameter is also noticeable, considering that, as the gap decreases, the extension of the central zone of the footprint increases at high speeds, though it is not so relevant as the impact of the working conditions.

For the tangential component (Fig. 14), the RMS maps have been pitch-averaged along the circumferential direction to obtain the representative values close to the tongue. In this case, the effect on the component is much more moderate, although it doubles in intensity between large and low gaps. In the case of the flow rate, it is more prominent for higher flow rates than for lower ones.

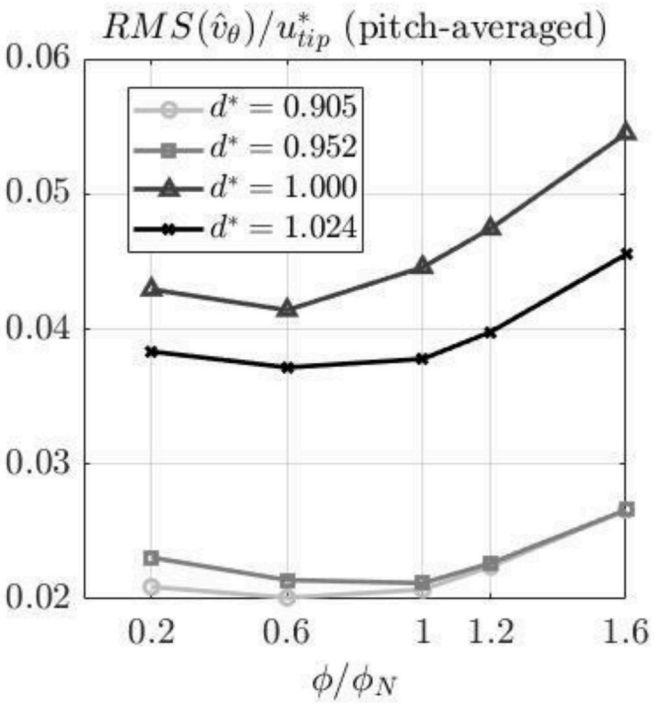

Fig. 14. Evolution of the maximum RMS values of the pure temporal term in the blade-to-blade midspan plane for the radial velocity. Impact of the off-design conditions and the radial gap size.

5. Conclusions

A detailed analysis of the deterministic flow variables, in terms of velocity components, has been completed in a centrifugal pump. A full 3D URANS numerical dataset, composed of 4 radial gap sizes between the impeller and the volute tongue and operated for 5 different flow conditions, has been considered for this purpose. The numerical model was already developed and used to validate the analysis of the pressure fluctuating field in the volute and several previous publications by the research group back its capability up regarding that dynamic fields' definition. Therefore, the main novelty of the paper is the special attention devoted to the impact of the radial clearance in the blockage phenomena and in the impact on the different components responsible for the establishment of unsteady flow sources. In particular, both radial and tangential velocities at the impeller outlet and in the inner meridional plane of the pump impeller have been intensively analyzed to foresee its impact on the pump operation and global variables: pressure distributions, flow rate, head and efficiency.

On the radial component, the observed unsteadiness in the centrifugal pump at low flow rates is mainly due to the pure temporal term and it is associated with the flow detachment on the pressure side of the blades that interacts strongly with the tongue. The radial gap between impeller and volute has no significant impact on this pattern. On the contrary, at high flow rates, the major unsteadiness lies in the rotating

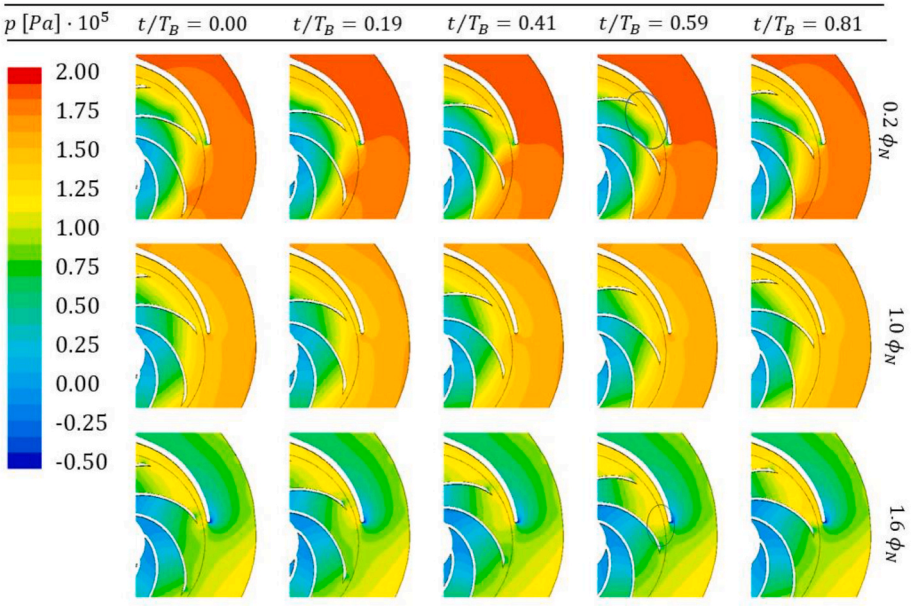

Fig. 13. Temporal evolution of the static pressure in the blade-to-blade midspan plane. Operating conditions effect for the impeller diameter d* = 1: 20% (up), 100% (center) and 160% (bottom) of Q_N.

blade-to-blade (spatial) component, due to the hydrodynamic load of the blades. The unsteady viscous interaction is manifested as flow velocity oscillations accounting for 40% of the time averaged value. Although the gap is not as important factor as the operating conditions for the pure rotor-stator interaction, it is promoting pulsations up to 1.5 times higher in case of radial gap reductions from 23.2% to 8.8% of the impeller diameter.

Regarding the tangential component, the contribution of the gap is relevant, showing more dispersion in the results. In this case, the spatial and temporal terms behave very similarly, increasing at off-design flow conditions, but being the spatial component significantly higher. In the spatial term, it is on the larger gap where there is less impact, with the maximum values concentrated in the trailing edge, while local fluctuations up to a 30% of the mean value can be observed for the reduced gap. Finally, in the temporal component (which also has the highest contributions in the trailing edge of the blades) the highest impeller-volute interaction is observed for the reduced gap size, representing roughly a 5–10%.

In view of these results, the oscillations in the flow blockage (linked to the radial component) are mainly due to flow structures in the impeller, with little contribution from the impeller-volute gap distance. Alternatively, oscillations in the available torque (associated to the circumferential component) are influenced by the impeller-tongue radial clearance and are more relevant at off-design flow rates.

Future work should analyze the deterministic stress tensor, its main diagonal, which is responsible for the deterministic kinetic energy and further comparison with the turbulence kinetic energy provided by the URANS modelling. Moreover, all these conclusions may help to advance in a more efficient selection of geometrical parameters, including the deterministic flow variables as objective functions for optimization.

Credit author statement

Fernández Oro, Jesús Manuel: Conceptualization, Methodology, Formal analysis, Visualization, Writing-Original draft preparation. Barrio Perotti, Raúl: Software, Resources, Data curation, Visualization, Writing-Original draft preparation. Galdo-Vega, Mónica: Investigation, Validation, Writing- Original draft preparation. González Pérez, José: Data curation, Writing- Reviewing and Editing, Supervision.

Declaration of competing interest

The authors declare that they have no known competing financial interests or personal relationships that could have appeared to influence the work reported in this paper.

Data availability

Data will be made available on request.

Acknowledgements

The authors gratefully acknowledge the financial support from Project ENE2017-89965-P provided by the Spanish Ministry of Economy, Industry and Competitiveness. It is also important and thanked the economic support of the “Agencia Estatal de Investigación” (AEI) of the Spanish Ministry of Science and Innovation, in the context of the State Program to Promote Scientific-Technical Research and its Transfer, through the Project “Optimization through flow control techniques of a vertical axis wind turbine for urban environments” (ref. TED2021-131307B–I00), included in the NextGenerationEU funds of the European Community. Additionally, the contribution of the University Institute for Industrial Technology of Asturias (IUTA), through projects SV-19-GIJON-1-15, SV-20-GIJON-1-17 and SV-22-GIJON-1-02, has allowed the development of this study.

References

[1] Waide P, Brunner C. Energy efficiency policy opportunities for electric motor-driven systems. International Energy Agency (OECD/IEA); 2011. https://www.iea.org/reports/energy-efficiency-policy-opportunities-for-electric-motor-driven-systems.
[2] De Almeida AT, et al. Improving the penetration of energy-efficient motors and drivers. Portugal: European Commission SAVE Study, Institute of Systems and Robotics, University of Coimbra; 2008.
[3] Capurso T, Bergamini L, Torresi M. Performance analysis of double suction centrifugal pumps with a novel impeller configuration. Energy Convers Manag X 2022;14:100227.
[4] US Department of Energy (DOE) and Hydraulic Institute. Improving pumping system performance. A sourcebook for Industry. https://www.energy.gov/sites/prod/files/2014/05/f16/pump.pdf; 2006.
[5] Kalaiselvan ASV, Subramaniam U, Shanmugam P, Hanigovszki N. A comprehensive review on energy efficiency enhancement initiatives in centrifugal pumping system. Appl Energy 2016;181:495–513.
[6] Neumann B. The interaction between geometry and performance of a centrifugal pump. London: Mechanical Engineering; 1991.
[7] Lakshminarayana B. An assessment of computational fluid dynamic techniques in the analysis and design of turbomachinery – the 1990 freeman scholar lecture. ASME J Fluids Eng 1991;113(3):315–52.
[8] Brennen CE. Hydrodynamics of pumps. New York: Oxford University Press and CETI Inc; 1994.
[9] González J, Fernández J, Blanco E, Santolaria C. Numerical simulation of the dynamic effects due to impeller-volute interaction in a centrifugal pump. ASME J Fluids Eng 2002;124(2):348–55.
[10] Barrio R, Blanco E, Parrondo J, González J, Fernández J. The effect of impeller cutback on the fluid-dynamic pressure pulsations and load at the blade-passing frequency in the volute of a centrifugal pump. ASME J Fluids Eng 2008;130(11):111102.
[11] Tsukamoto H, Uno M, Hamafuku H, Okamura T. Pressure fluctuation downstream of a diffuser pump impeller. In: 2nd Joint ASME/JSME Fluids Engineering Conference, vol. 216; 1995. p. 133–8.
[12] Dong R, Chu S, Katz J. Effect of modification to tongue and impeller geometry on unsteady flow, pressure fluctuations and noise in a centrifugal pump. ASME J Turbomach 1997;119(3):506–15.
[13] Croba S, Kueny JL. Numerical calculation of 2D, unsteady flow in centrifugal pumps: impeller and volute interaction. Int J Numer Methods Fluid 1996;22(6):467–81.
[14] Shi F, Tsukamoto H. Numerical study of pressure fluctuations caused by impeller-diffuser interaction in a diffuser pump stage. ASME J Fluids Eng 2001;123(3):466–74.
[15] Goto A, Zangeneh M. Hydrodynamic design of pump diffuser using inverse design method and CFD. ASME J Fluids Eng 2002;124(2):319–28.
[16] Barrio R, Parrondo J, Blanco E. Numerical analysis of the unsteady flow in the near-tongue region in a volute-type centrifugal pump for different operating conditions. Comput Fluid 2010;39:859–70.
[17] Plugiese F, De Paola F, Fontana N, Giugni M, Marina G. Experimental characterization of two Pumps as Turbines for hydropower generation. Renew Energy 2016;99:180–7.
[18] Shojaeefard MH, Tahani M, Ehghaghi MB, Fallahian MA, Beglari M. Numerical study of the effects of some geometric characteristics of a centrifugal pump impeller that pumps a viscous fluid. Comput Fluid 2012;60:61–71.
[19] Yousefi H, Noorollahi Y, Tahani M, Fahimi R, Saremian S. Numerical simulation for obtaining optimal impeller's blade parameters of a centrifugal pump for high-viscosity fluid pumping. Sustain Energy Technol Assessments 2019;34:16–26.
[20] Deng S, Li G, Guan J, Chen X, Liu L. Numerical study of cavitation in centrifugal pump conveying different liquid materials. Results Phys 2019;12:1834–9.
[21] Wu C, Pu K, Li C, Wu P, Huang P, Wu D. Blade redesign based on secondary flow suppression to improve energy efficiency of a centrifugal pump. Energy 2022;246:123394.
[22] Lin Y, Li X, Zhu Z, Wang X, Lin T, Cao H. An energy consumption improvement method for centrifugal pump based on bionic optimization of blade trailing edge. Energy 2022;246:123323.
[23] Ji L, Li W, Shi W, Chang H, Yang Z. Energy characteristics of mixed-flow pump under different tip clearances based on entropy production analysis. Energy 2020;199:117447.
[24] Wang Z, Qian Z, Lu J, Wu P. Effects of flow rate and rotational speed on pressure fluctuations in a double-suction centrifugal pump. Energy 2019;170:212–27.
[25] Sonawat A, Kim S, Ma S-B, Kim S-J, Lee JB, Yu MS, J-H K. Investigation of unsteady pressure fluctuations and methods for its suppression for a double suction centrifugal pump. Energy 2022;252:124020.
[26] Adamczyk JJ. Aerodynamic analysis of multistage turbomachinery flows in support of aerodynamic design. ASME J Turbomach 2000;122(2):189–217.
[27] Leboeuf F. Unsteady flow analysis in transonic turbine and compressor stages. In: VKI Lecture series 2002-01 on recent development in numerical methods for turbomachinery flows; 2002.
[28] Fernández Oro JM, González J, Argüelles KM, Guerras FI. Decomposition of deterministic unsteadiness in a centrifugal turbomachine: non-linear interactions between the impeller flow and volute for a double suction pump. ASME J Fluids Eng 2011;133(1):011103.
[29] Fernández Oro JM, González J, Barrio Perotti R, Galdo Vega M. Numerical analysis of the deterministic stresses associated to impeller-tongue interactions in a single volute centrifugal pump. ASME J Fluids Eng 2019;141(9):091104.

[30] Parrondo JL, González J, Fernández J. The effect of the operating point on the pressure fluctuations at the blade passing frequency in the volute of a centrifugal pump. ASME J Fluids Eng 2002;124:784–90.
[31] González J, Parrondo J, Santolaria C, Blanco E. Steady and unsteady radial forces for a centrifugal pump with impeller to tongue gap variation. ASME J Fluids Eng 2006;128(3):454–62.
[32] Morgenroth M, Weaver DS. Sound generation by a centrifugal pump at blade passing frequency. ASME J Turbomach 1998;120:736–43.
[33] Parrondo J, Pérez J, Barrio R, González J. A simple acoustic model to characterize the internal low frequency sound field in centrifugal pumps. Appl Acoust 2011;72 (1):59–64.
[34] Keller J, Parrondo J, Barrio R, Fernández J, Blanco E. Effects of the pump-circuit acoustic coupling on the blade-passing frequency perturbations. Appl Acoust 2014; 76:150–6.